

## **Indigenous Microbiota Protects against Inflammation-Induced Osteonecrosis**

D.W. Williams, H.E. Vuong, S. Kim, A. Lenon, K. Ho1 E.Y. Hsiao, E.C. Sung, and R.H. Kim

### **Appendix**

#### **Supplemental Methods**

##### Micro-computed tomography

Whole maxillae and femurs were scanned with a voxel size of  $10 \mu\text{m}^3$  using a 1.0 mm aluminum filter at 60 kVp and 166  $\mu\text{A}$  (SkyScan 1275; Bruker). 2-dimensional images were reconstructed using N Recon (Bruker) following X-Y alignment and dynamic range adjustment. Reconstructed images were used for bone loss analysis (maxillae) or trabecular bone morphometry (femur). Bone loss was quantified by measuring the distance between cementoenamel junction and the alveolar ridge on the palatal, mesiobuccal and distobuccal roots of M2 using CTAn (Bruker). Trabecular measurements were performed on the distal femur and reported in accordance to published guidelines (Bouxsein et al. 2010). 3-dimensional representative images were generated in CTVox (Bruker).

##### Quantitative real-time PCR

Bacterial DNA was extracted from weighed fecal and oral samples of two randomly selected animals per cage in both SPF and Abx groups taken before sacrifice using the DNeasy PowerSoil Kit (Qiagen; #12888-100). Total bacterial load was performed using a standard curve constructed from known quantities of 16S rDNA from *Porphyromonas gingivalis* (FDC 381). PCR reactions were performed in duplicate and were carried out in a 7500 Real-Time PCR system (ThermoFisher Scientific). Total bacterial load was divided by the weight of the starting material for each sample.

##### 16S sequencing and quantitative real-time PCR

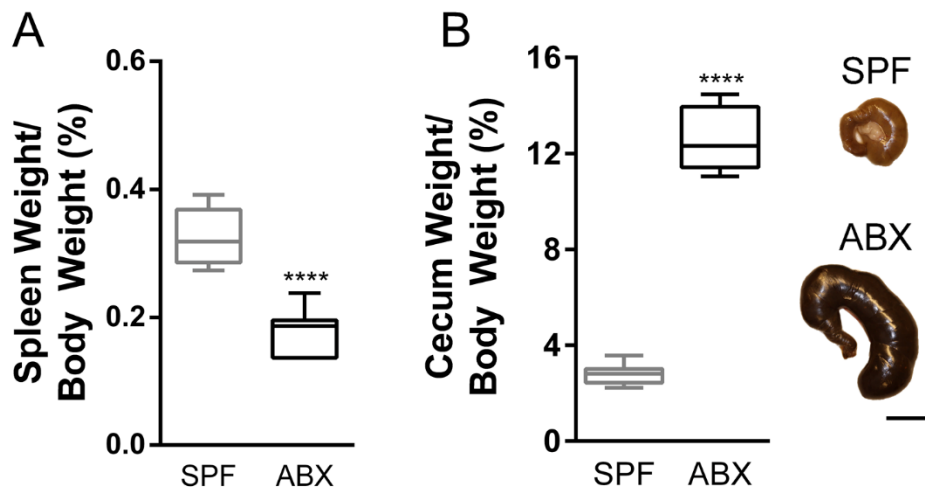
Bacterial DNA underwent library preparation as described (Tong et al. 2014) using uniquely barcoded primers targeting the V4 region of the 16S rRNA gene (Caporaso et al. 2012). Pooled libraries diluted to 6pM in 20% PhiX underwent paired-end (2x250bp) sequencing using the Illumina MiSeq v2 platform. Demultiplexed sequencing results were analyzed with the QIIME2 pipeline (Bolyen et al. 2019). Following paired end sequence joining and quality control, samples were denoised and clustered using the deblur function. Sequences were aligned and a tree was constructed for phylogenetic diversity analyses. Community richness was determined using Faith's Phylogenetic Diversity and compared between groups using an unpaired t-test. Alpha rarefaction plots were generated to determine alpha diversity as a function of sampling depth and significance was determined with an unpaired t-test. Bray-Curtis dissimilarity calculations were performed to determine community dissimilarity and principal coordinates analysis plots were visualized in Emperor. Beta distances were calculated and compared between SPF and Abx using a pairwise PERMANOVA test. Taxonomic composition of the samples was performed using a pre-trained naïve Bayes classifier, trained with Greengenes 13\_8 99% OTUs, where reference sequences were trimmed in the same way as sample sequences to include 250 bases from the sequenced region of the 16S gene (V4 region bound by 515F/806R primers). Differentially abundant microbes between SPF and Abx cohorts were determined using discrete false-discovery rate (Jiang et al. 2017).

#### *In vitro* osteoclast culture and functional assay

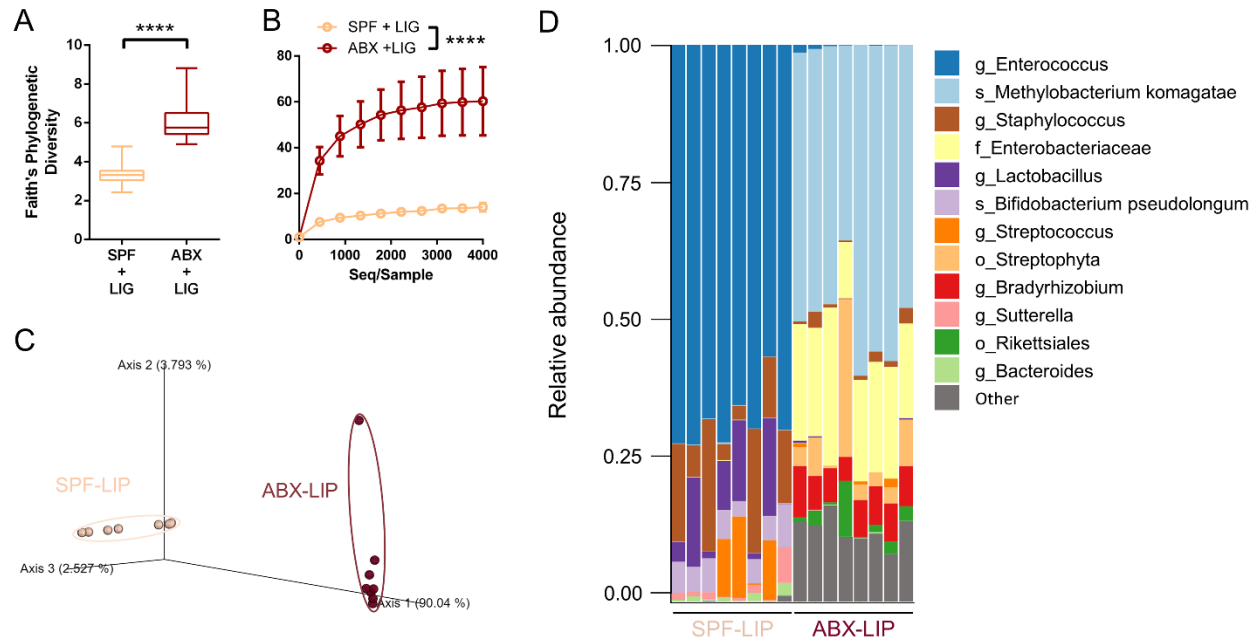
Bone marrow cells (BMC) were isolated from the femurs and tibia of SPF and Abx mice by flushing with basal media (minimal essential media, 10% v/v glutamate, 10% v/v fetal bovine serum, and 100U/mL penicillin/streptomycin), and passing cells through a 70µm filter. Cells were counted and 200,000 cells were seeded per well to assess osteoclast characteristics in

culture or 10,000 cells per dentin slice to assess osteoclast functional activity. BMC were differentiated to macrophages by supplementing basal media with 10nM M-CSF for 3 days. After 3 days, cells were incubated in basal media supplemented with 10nM M-CSF and 10nM RANKL for 5 days until large, multinucleated osteoclasts formed. For osteoclast characterization, osteoclasts were fixed and stained with TRAP (#387A-1KT, Millipore Sigma), imaged with a brightfield microscope and quantified with ImageJ. For osteoclast functional assay, dentin slices were stained with hematoxylin following osteoclast detachment with a cotton swab. Hematoxylin stain was quantified using the Colour Deconvolution plugin in ImageJ.

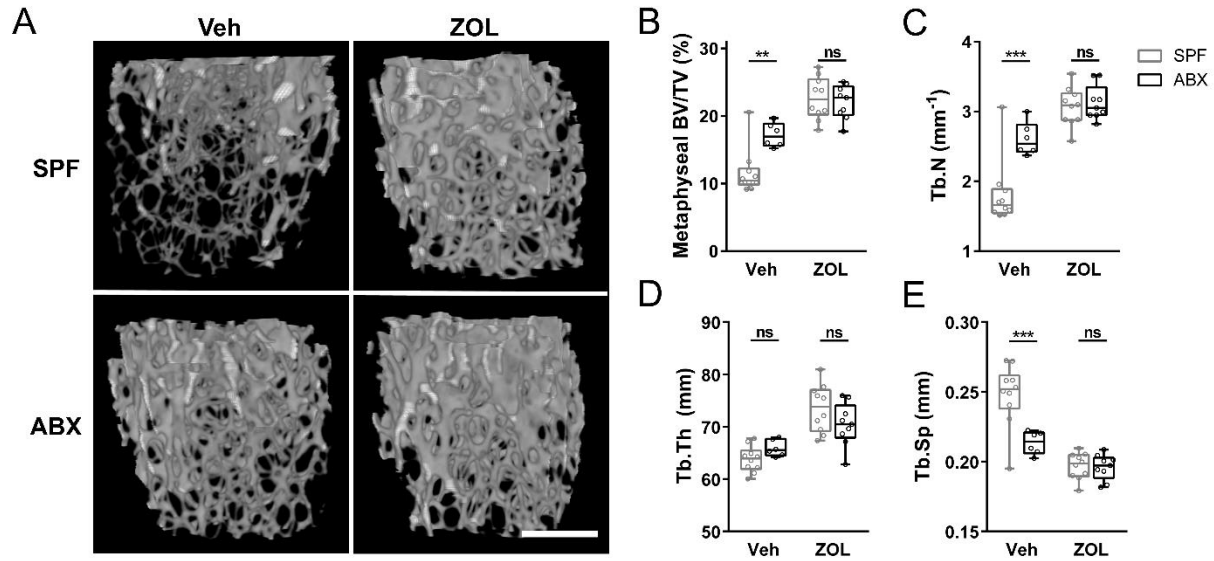
**Appendix Figures:**



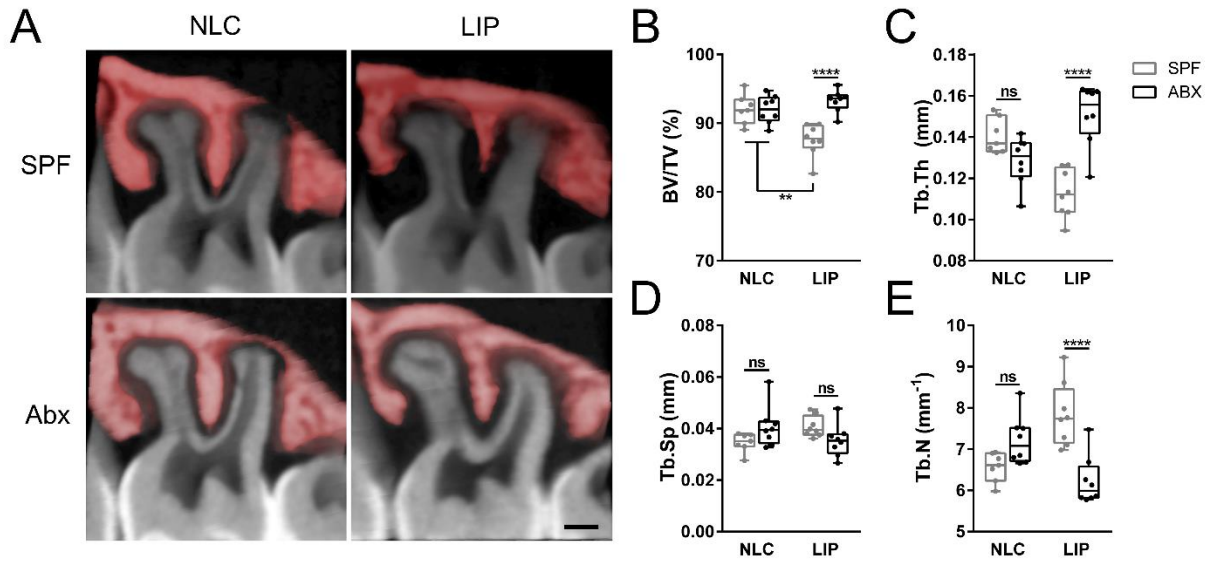
**Appendix Figure 1.** Spleen (A) and cecum (B) weights are presented as a percentage of total animal body weight at the time of sacrifice. Representative images of ceca from SPF and Abx groups on the far right. Scale bar: 10mm.



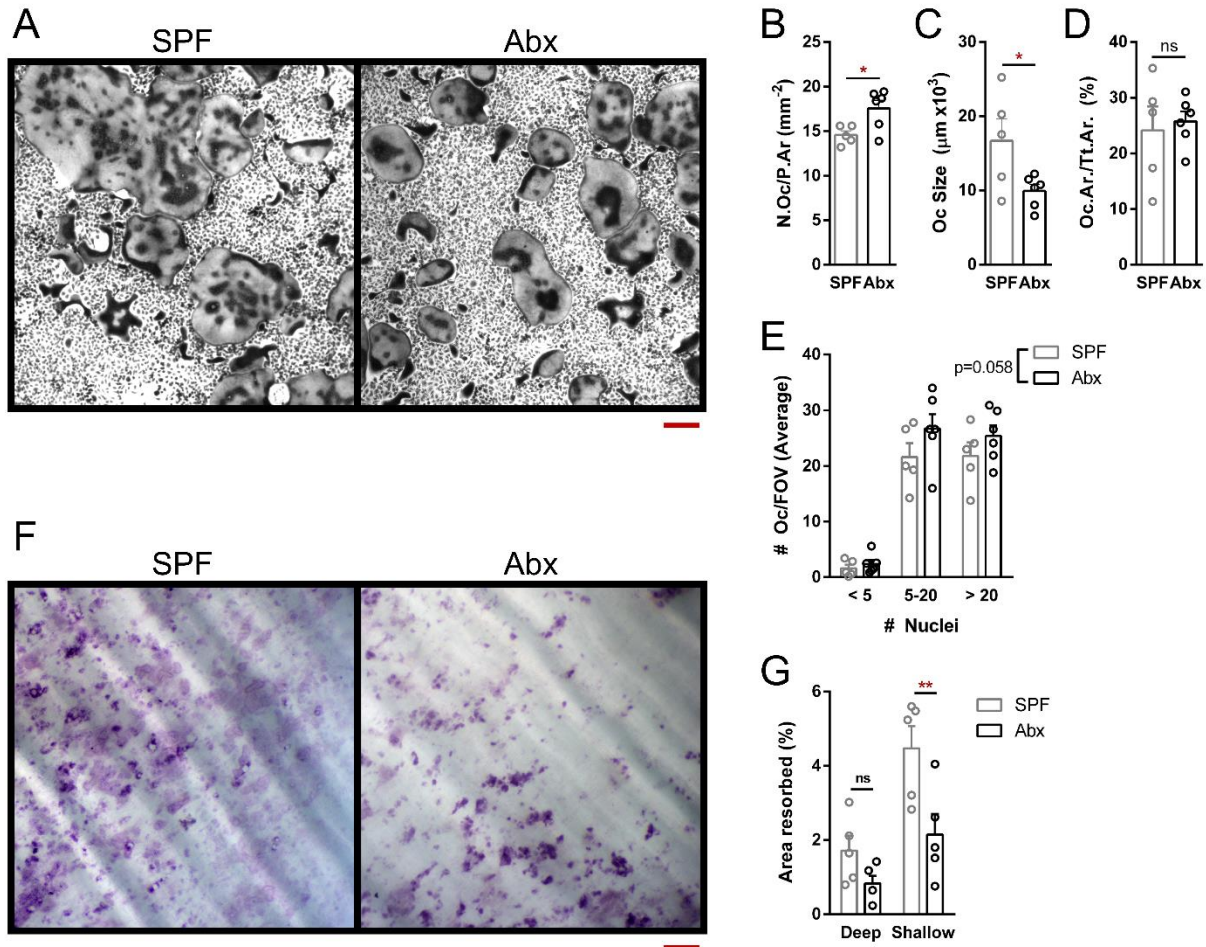
**Appendix Figure 2.** The alpha (A, B) and beta (C) diversity of the microbial communities present on the ligature were calculated by Faith's phylogenetic diversity, alpha rarefaction plot, and Bray-Curtis dissimilarity principal component analysis, respectively. D) Microbiome composition is shown at the operational taxonomic unit (OTU) level. The top 12 OTUs are classified at the highest taxonomic level identified. s\_, species; g\_, genus; f\_, family. LIP, ligature-induced periodontitis. \*\*\*\* p < 0.0001. Quantified data is presented as a min/max box and whisker plot (A) or mean  $\pm$  SD (B).



**Appendix Figure 3.** (A) Representative images of the metaphyseal trabecular bone from the distal femur. Scale bar: 500 $\mu$ m. B-E. Quantification of bone mass (B), trabecular number (C), trabecular thickness (D), and trabecular separation (E) measured from the region pictured in (A). SPF, specific pathogen free; Abx, antibiotic treated; Veh, vehicle; ZOL, zoledronic acid; BV/TV, bone mass percentage; Tb.N, trabecular number; Tb.Th, trabecular thickness; Tb.Sp, trabecular separation. Quantified data is presented as min/max box and whisker plots. ns, not statistically significant; \*\*  $p < 0.01$ ; \*\*\*  $p < 0.001$ .



**Appendix Figure 4.** (A) Graphical representation of bone included in bone mass quantification at the buccal roots of the second maxillary molar. Bone included in analysis is pseudocolored in red. Scale bar: 200 $\mu$ m. B-E. 3-dimensional bone morphometric properties of buccal bone in (A) including bone mass (B), trabecular thickness (C), trabecular separation (D) and trabecular number (E). SPF, specific pathogen free; Abx, antibiotic-treated; NLC, non-ligature control; LIP, ligature-induced periodontitis; BV/TV, bone volume per tissue volume; Tb.Th, trabecular thickness; Tb.Sp, trabecular separation; Tb.N, trabecular number. Quantified data is presented as min/max box and whisker plots. ns, not statistically significant; \*\*  $p < 0.01$ ; \*\*\*\*  $p < 0.0001$ .



**Appendix Figure 5.** (A) Representative image of TRAP staining on bone marrow macrophages (BMMs)-derived osteoclasts obtained from SPF-treated or Abx-treated mice. Cells are allowed to differentiate into osteoclasts in the presence of M-CSF (10<sup>4</sup>U/ml) and RANKL (100 ng/ml). Scale bar: 100µm. Quantification of cultured osteoclast properties, including number of osteoclasts per area (B), average osteoclast area (C), total osteoclast area (D) and osteoclasts stratified by TRAP+ nuclei (E). F. Representative images of the osteoclast activity assay (violet color represents resorption). G. Areas of deep (dark violet) or shallow (light violet) resorption were quantified. Scale bar: 100µm. All quantified data represent mean ± SEM. ns, not statistically significant; \* p < 0.05; \*\* p < 0.01.

## Appendix References

- Bolyen E, Rideout JR, Dillon MR, Bokulich NA, Abnet CC, Al-Ghalith GA, Alexander H, Alm EJ, Arumugam M, Asnicar F et al. 2019. Reproducible, interactive, scalable and extensible microbiome data science using qiime 2. *Nat Biotechnol.* 37(8):852-857.
- Bouxsein ML, Boyd SK, Christiansen BA, Guldberg RE, Jepsen KJ, Muller R. 2010. Guidelines for assessment of bone microstructure in rodents using micro-computed tomography. *Journal of bone and mineral research : the official journal of the American Society for Bone and Mineral Research.* 25(7):1468-1486.
- Caporaso JG, Lauber CL, Walters WA, Berg-Lyons D, Huntley J, Fierer N, Owens SM, Betley J, Fraser L, Bauer M et al. 2012. Ultra-high-throughput microbial community analysis on the illumina hiseq and miseq platforms. *ISME J.* 6(8):1621-1624.
- Jiang L, Amir A, Morton JT, Heller R, Arias-Castro E, Knight R. 2017. Discrete false-discovery rate improves identification of differentially abundant microbes. *mSystems.* 2(6).
- Tong M, Jacobs JP, McHardy IH, Braun J. 2014. Sampling of intestinal microbiota and targeted amplification of bacterial 16s rna genes for microbial ecologic analysis. *Curr Protoc Immunol.* 107:7 41 41-11.